Egypt. J. Chem. Vol. 65, No. 11 pp. 707 -725 (2022)

Egyptian Journal of Chemistry

http://ejchem.journals.ekb.eg/

Assessment of Cytotoxicity and Genotoxicity Response of Zinc Sulphate on Eukaryotic Cells

Shimaa A. A. Mousa[a*], Abd El-Hamid A Haggran[a], Tahany M.A El-Kawokgy[a], Zakia A. Abo El-Kheir[b], Shadia M. H. Sabry[b], and Shimaa E. Rashad[a]

[a] *Microbial Genetics Department, Biotechnology Research Institute, National Research Centre, Giza, Egypt.*

[b] *Botany and Microbiology Department, Faculty of Science, AL- Azhar University, Cairo, Egypt*

Abstract

A chemical called zinc sulphate ($ZnSo_4$) is inorganic. In order to treat and prevent nutrient deficiencies, zinc is utilised. Zinc is a naturally occurring element that is crucial for tissue development, maintenance, and health. This research used the MTT method to examine the effects of various doses of $ZnSo_4$ on cell viability in hepatocellular carcinoma (HepG2), lung cancer (A549), and normal lung cells (Wi38). Propidium iodide (PI) staining and Annexin V/PI staining were used in flow cytometry to detect both apoptosis and cell cycle arrest appropriately. The current study's findings revealed that $ZnSo_4$ caused cytotoxicity in HepG2, A549, and Wi38 at various doses (IC50 = 308.11, 413.02, and 463.15 g/ml). These findings demonstrated that $ZnSo_4$ has cytotoxic effects on both cancerous and non-cancerous cells by reducing cell viability. By arresting the cell cycle in the G2/M phase and increasing apoptosis, flow cytometry analysis of $ZnSo_4$-damaged HepG2 cells revealed a considerable increase in these two processes. In addition, when HepG2 cell lines were exposed to a high concentration of $ZnSo_4$, the mRNA expression amounts of *p53* and *casp3* rose whereas *Bcl-2* fell. This study assessed how $ZnSo_4$ affected various yeast haploid knockout strains (YKO). In order to determine the three different $ZnSO_4$ concentrations that this particular set of $ZnSO_4$ could cause DNA damage, we used the comet assay method. The comet assay showed improved yeast cell sensitivity, which has been unquestionably confirmed. The (Clustal Omega Multiple Sequence Alignment EMBL-EBI) alignments of yeast and human gene sequence similarity were used to select the genotypes of YKO.

Keywords: *Zinc Sulphate, cell lines, flow cytometry, apoptosis, RT-PCR, Comet assay.*

Introduction

Zinc is a necessary trace element with significant biological functions that regulate numerous cellular processes, including protein biosynthesis, DNA synthesis, healthy growth, brain development, behavioural response, foetal development, and bone metabolism (**Yehy *et al.*, 2011**). It also regulates the response to insulin, reproduction, antioxidant cellular defence systems, and reproduction (**Klug, 2010**).

Zinc works best at very low amounts, therefore an abundance of it in body fluids could be hazardous (**Barbier *et al.*, 2005**). As a cofactor for more than 300 enzymes, zinc is a key trace element needed for numerous signalling pathways in the human body. These enzymes are involved in cell metabolism, cell proliferation, and other cellular processes (**Costello and Franklin 2016**). Furthermore, zinc is poisonous to cells at high doses and promotes a number of intracellular processes that lead to the production of reactive oxygen species (ROS) (**McCord and Aizenman 2018**).

Znic was applied to various cell types at concentrations ranging from 25 to 300 M, and the degrees of cytotoxicity and genotoxicity were highly variable (**Sliwinski *et al.*, 2009** and **Plum *et al.*, 2010**). According to **Nazrolu and Yürekli (2013)**, zinc deficiency increases sensitivity to oxidative stress, which may, in part, raise the chance of developing cancer (**Silvera and Rohan 2007**) However, too much zinc can cause DNA double-strand breaks and chromosomal instability in human lung cells (**Xie *et al.*, 2009**).

As shown by **Zaman *et al.*, 2019,** CK2 regulates zinc homeostasis in breast and prostatic cancer cells as TBB and CX-4945 significantly reduced cell viability following exposure to zinc. On *in vitro* human cell growth, cytotoxicity and programmed cell death (apoptosis) were investigated. Genes associated with apoptosis and cell cycle arrest was also examined in the human cell lines **(Rashad *et al.*, 2018).** The fact that cadmium chloride reduced therapeutic effectiveness in cancerous cells at relatively modest levels as compared to non-cancerous cells further demonstrated the metal's anticancer capabilities (**Mousa *et al.*, 2022**).

*Corresponding author e-mail: sa.mousa@nrc.sci.eg.; (Shimaa A. Mousa).
Received Date; 30 May 2022; Revise Date: 07 June 2022; Accept Date: 09 June 2022.
DOI: 10.21608/ejchem.2022.141668.6209

Rashad *et al.*, 2019 found that certain chemicals found in food decreased cell proliferation in both cancerous and non-cancerous cells, confirming the substances' cytotoxic effect and demonstrating that *Saccharomyces cerevisiae* cells were more sensitive to them**.** To establish the ideal concentrations at which this combination of dietary chemicals could lead to DNA damage, the comet assay was employed to examine the effects of chemicals on several yeast haploid knockout strains (**Rashad *et al.*, 2021**).

Flow cytometric investigation showed that AuNRs has a cytotoxic influence on human cell lines (HepG2, CaCo2, A549, and CDD-19Lu) repeated through the enhanced G2/M phase cell cycle arrest. AuNRs has a cytotoxic activity on both carcinoma and normal cells (**Rashad *et al.*, 2022**). The in culture nephrotoxicity of zinc sulphate heptahydrate $ZnSo_4$ 7H2O was examined by **Marcináková *et al.*, 2019** utilising rabbit epithelial kidney cells RK13 as the model cell line.

According to their research, the MTT test's MTT inhibitory concentration IC50 value for xCELLigence monitoring was 101.8 mg/l. Reduced cell viability at a high dose (100 M) (**Zhang *et al.*, 2017**). $ZnSo_4$ effects at a particular concentration range on MDAMB231, HepG2, and 293 T cell line viability, cell cycle, and apoptosis as measured by flow cytometry. It was discovered that $ZnSo_4$ had diverse effects on cell cycle, apoptosis, and cell viability in different cell lines, each of which corresponded to changes in Zn^{2+} level in the three cell lines.

Cell death, an arrest in the G1 and G2/M cell cycles, and an increase in the apoptosis proportion were all caused by the MDAMB231 cells' intracellular zinc content's considerable rise. Interestingly, when the three cell lines were exposed with a high concentration of $ZnSo_4$, the rates of expression pattern of the ZnT and ZIP families increased and decreased in accordance with, alternately, their roles (**Wang *et al.*, 2013**).

Materials and methods

1. Cell lines

1.1. **Mammalian cell lines: HepG-2** cells Wi38 cells (human lung fibroblast normal cells), A-549 (cell lines cancer), and (human liver cancerous cells line) have been obtained from the American Type Gene Bank (ATCC, Rockville, MD).

Chemicals obtained from Sigma include dimethyl sulfoxide (DMSO), MTT, and trypan blue dye (St. Louis, Mo., The following products were purchased from Lonza: foetal bovine serum, RPMI-1640, HEPES buffer solution, L-glutamine, gentamycin, and 0.25% Trypsin-EDTA (Belgium).

1.2. **Cell line Propagation:**

On DMED medium supplemented with 10% inactivated foetal calf serum,1% L-glutamine and 50 µg/ml gentamycin, the cells have been cultured. The cells were subcultured two to three times per week and kept at 37 °C in a humidified environment with 5% CO2.

1.3. **Cytotoxicity evaluation using MTT assay:**

In Corning 96-well tissue culture plates, the tumour cell lines were suspended in media at a concentration of $5x10^4$ cells/well and then incubated for 24 hours. The 96-well plates were then filled with the $ZnSo_4$ ratios (three replicates). As a control, 0.5% DMSO was USA). used in each 96-well plate.

The MTT test was used to assess the number of cells that survived after 24 hours of incubation. The 96-well plates' media were briefly removed, and 100 µl of new culture DMEM medium without phenol red was substituted. Then, 10 µl of the 12 mM MTT stock solution (5 mg of MTT in 1 mL of PBS) was added to each well, including the untreated controls. The 96-well plates were then incubated for 4 hours at 37°C with 5% CO2. After removing an 85µl aliquot of the media from each well, 50 µl of DMSO was applied to each well, carefully blended with both the pipette, and then incubated at 37°C for 10 min.

The optical density was then assessed using a microplate reader at 590 nm (Sun Rise, TECAN, Inc, USA) Calculate the percentage of viability and the quantity of viable cells using the formula [(ODt/ODc)]. x100 where ODt is the average optical density of the test sample-treated wells. The mean optical density of untreated cells is known as ODc. To determine the survival curve of each tumour cell line following treatment with the chosen chemical, the relationship between surviving cells and $ZnSo_4$ concentrations is shown. Utilizing Graph Pad Prism software (San Diego, CA, USA), the 50% suppressive concentration (IC50), or the amount needed to have harmful effects in 50% of intact cells, was calculated from graphic plots of the dose response curve for each concentration (**Rashad *et al.*, 2022**).

2. Flow cytometry

2.1. Cell cycle analysis by PI assay using flow cytometry

The cells were degraded for 10 minutes at 37°C with warm Trypsin-EDTA and warm Phosphate Buffered Saline (PBS)-Ethylene diamin tetra acetate (EDTA) (0.25%). The supernatant was carefully removed after the mixture was centrifuged at 450 rpm for 5 minutes. After two warm PBS washes the cell pellet was re-suspended in 500 µl of warm PBS, centrifuged, and the supernatant was drained.

To fix the cells, 350 µl of ice-cold 70% ethanol and 150 µl of PBS were combined and kept at 4°C for an hour. The mixture was centrifuged at 350 rpm for 10 minutes to remove the ethanol before carefully removing the

supernatant. Two warm PBS washes were performed on the mixture, and the cells were then re-suspended in 500 µl of warm PBS before centrifuging the mixture and removing the supernatant. The cells were re-suspended in 100 µl of PBS and kept at 4 °C in the dark for up to 4 days. The cells were stained for 30–60 minutes in the dark using 100 µl of PI (Propidium Iodide) solution and 50 µl of RNase A solution (100 µg/ml) (**Rashad *et al.*, 2022**). In Attune flow cytometry, the labelled cells were read (**Applied Bio-system, USA**).

2.2. **Apoptosis analysis by Annexin V-FITC Assay using flow cytometry**

Centrifuging, $1–5\times10^5$ cells were collected, and the supernatant was discarded. After that, cells were collected, twice-washed in warm PBS buffer, and thereafter re-suspended in 500 µl of 1X Binding Buffer. Propidium iodide (PI) 50 mg/ml and 5 µl of Annexin V-FITC should be added, and the mixture should then be incubated at room temperature for 5 minutes in the dark (**Vermes *et al.*, 1995**). Utilize flow cytometry to examine Annexin V-FITC binding (**Applied Bio-system, USA**).

3. Quantitative RT-PCR analysis

Using the Gene JET RNA Purifying Kit (Thermo Scientific, # K0731, USA), total RNA was extracted from HepG2 cells in accordance with the manufacturer's instructions. To create cDNA, total RNA (5 µg) was reverse synthesized using Revert Aid H Minus Reverse Transcriptase (Thermo Scientific, #EP0451, USA) (**Rashad *et al.*, 2018**). Using the Step One Plus real time PCR technology, the relative expression of the genes involved to apoptosis was determined using the cDNA as a template (Applied Bio system, USA). Primer 5.0 software was used to create the primers. *Casp3, Bcl-2, p53*, *GAPDH*, and their forward and reverse primer sequences are listed in a flowing table (1).

Table (1): Forward and reverse primer sequences *for Casp3, Bcl-2, p^{53}*, and *GAPDH* genes.

Gene	Forward primer (5' ----- 3')	Reverse primer (5' ----3')
Casp3	TTCATTATTCAGGCCTGCCGAGG	TTCTGACAGGCCATGTCATCCTC
Bcl-2	CATGCAAGAGGGAAACACCAGA	GTGCTTTGCATTCTTGATGAGGG
p^{53}	AGAGTCTATAGG CCACCCC	GCTCGACGCTAGGATCTG AC
GAPDH	TGCACCACCAACTGCTTAGC	GGCATGGACTGTGGTCATGAG

The fold change in target gene expression was calculated using the housekeeping gene *GAPDH* as a reference. 12.5 µl of 2X Maxima SYBR Green/ROX qPCR MM (Thermo Scientific, # K0221, USA), 2 µl of cDNA template, 1 µl of forward primer, 1 µl of reverse primer, and 8.5 µl of nuclease-free water were combined to create a 25 µl PCR mix. Thermal cycling settings were as follows: initial DNA denaturation at 95 °C for 10 min, followed by 40–45 cycles of DNA amplification at 95 °C for 15 s, followed by annealing at 60 °C for 30 s and extension at 72 °C for 30 s. For melting curve analysis, the temperature was raised from 63 to 95°C at the conclusion of the previous cycle. Intended genes' cycle threshold (Ct) ratios and the housekeeping gene's proportional gene expression

4. Yeast Comet assay (YCA)

Utilizing the first method described in the publication by (**Rashad *et al.*, 2021**). We employed yeast culture media with 50, 75, and 100 µg/ml of $ZnSO_4$. Additionally, a medium devoid of chemical components was used as an untreated control. Cold PBS was added to a one-cubic-centimeter container along with one gramme of cell pellets.

After swirling this suspension for five minutes, it was filtered. A total of 600 ml of low-melting agarose and 100 µl of cell suspension were combined (0.8 percent in PBS).This mixture was evenly distributed across all of the slides that had already been coated. The coated slides were submerged in lyses buffer (0.045 M TBE, pH 8.4, containing two 0.5% SDS) for fifteen minutes. The slides were put in an activity chamber without SDS but with the same TBE buffer. At 4 °C with a 2 V/cm electric field, the coated slides were put in the electrophoresis tank with electrophoresis buffer for 15 minutes. Neutralise the micro gels for 10 minutes with a neutralisation buffer at room temperature. Drain samples from neutralising buffer and soak them for 10 minutes at room temperature in 76% and 96% ethanol, respectively. Each slide was stained with 50 µl of 20 mg/m1 ethidium bromide. While the samples were still wet, the visible radiation magnifier was used to assess the migration patterns of 100 cells for each exposure level (With excitation filter 420-490nm [issue 510 nm]). To count and gauge the size of the comet, the tail lengths of were measured using in vitro $2^{-\Delta\Delta Ct}$ method **(Livak and Schmittgen, 2001).** Interplanetary objects were estimated from the nucleus to the top of the tails with a 40x increase. To see polymer damage, observations of Gel Red-stained polymer were made using a fluorescence magnifier and a 40x objective. Five image analysis code created by Kinetic Imaging, Ltd. In order to evaluate the quantitative and qualitative severity of polymer injury within the cells, (Liverpoo1, UK) linked to a CCD camera was utilised. The tail moment was then computed by the software. In the majority of cases, fifty to one hundred randomly chosen cells per sample were assessed in accordance with (**Rashad *et al.*, 2021)**.

5. Toxicity to (YKO) strains tested with Zink sulphate by comet assay

5.1. Knockout yeast strains of choice

In this study, haploid knockout strains with completely different genotypes were employed, and each strain's

sequences were chosen and aligned with the NCBI's database of human sequences (The National Centre for Biotechnology Information). To match the yeast genes used in this study, four genes that coincide with human genes related to cancer were selected (Table 2).

5.2. Selection of yeast haploid strains deficient in genes similar to human cancer genes

According on (Clustal Omega Multiple Sequence Alignment EMBL-EBI) needs to be aligned between human and yeast sequence similarities, the genotypes of yeast haploid (knockout) strains were selected Table (2).

Table (2): Selected yeast proteins which matched with cancer related human genes.

Selected strains	Selected genes of yeast strains (genotypes)	Homologous genes in human
YMR177W	MMT1	SLC30A9
YMR199W	CLN1	CCNA1
YMR224C	MRE11	MRE11
YMR243C	ZRC1	SLC30A10

5.3. Protein-protein interaction prediction

The interaction network was used in line with the order. GeneMANIA is a flexible, user-friendly web tool for analysing sequence collections, prioritising genes for particular studies, and assessing gene function theories.

Sources of information

Co Co-expression data from the Organic Phenomenon Omnibus (GEO), data on physical and genetic interactions from Bio GRID, information on predicted macromolecule interactions supported by orthology from I2D, and pathway and molecular interaction data from Pathway Commons, which combines information from Bio GRID, Memoria, and Pathway Commons. The human protein-protein interaction network and the network of interactions between proteins in yeast.

6. Statistical analysis

Every piece of data was expressed as means + S.D. One-way analysis of variance (ANOVA using SPSS 18.0 software, 2011) was used to assess the statistical significance, and Duncan's multiple ranged test was used to determine individual comparisons (DMRT). When p0.05, values were deemed statistically significant.

Results

1. Cytotoxic effect by MTT assay

Using the MTT cytotoxic assay, zinc sulfate's cytotoxic action was demonstrated at various doses on the proliferation of HepG2, A549, and Wi38 cells in comparison to a positive control.

As zinc sulphate concentrations rose, cell viability generally declined gradually, as seen in Table (3). As the measured zinc Sulphate concentration grew, the cytotoxicity increased and the viability of treated cells decreased. The dose that causes a 50% reduction in cell growth (IC50) in hepatoma cell line cells (HepG2) was found at dosimetric curves for viable cells to be 308.11 µg/ml. in Figure (1).

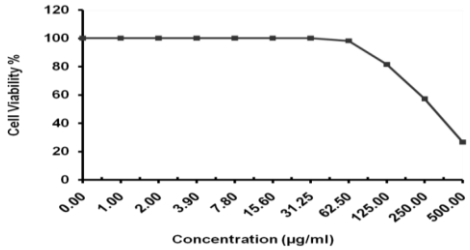

Figure 1: Inhibitory activity of $ZnSo_4$ concentrations against Hepatocellular carcinoma cells (HepG2)

Table (3). Effect of different $ZnSo_4$ concentrations on hepatocellular carcinoma cells (HepG2)

$ZnSo_4$ conc. (µg/ml)	Viability %	Inhibitory %	S.D. (±)
500	**34.68**	**65.32**	**2.34**
250	**78.94**	**21.06**	**2.82**
125	**94.03**	**5.97**	**1.75**
62.5	**99.26**	**0.74**	**0.48**
31.25	**100**	**0**	
15.6	**100**	**0**	
7.8	**100**	**0**	
3.9	**100**	**0**	
2	**100**	**0**	
1	**100**	**0**	
0	**100**	**0**	

As the quantities of zinc sulphate grew, the cell viability steadily reduced, as shown in Table (4). As the measured zinc Sulphate concentration grew, the cytotoxicity increased and the viability of treated cells decreased. At dose-response curves for cell viability, the dose inducing 50% cell growth inhibition (IC50) against lung cell lines (A549) was 413.02 µg/ml in Figure (2).

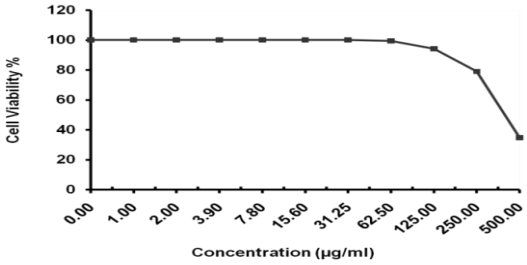

Figure 2: Inhibitory activity of ZnSo4 concentrations against lung carcinoma cells (A549)**.**

Table (4). Effect of different ZnSo4 concentrations on lung carcinoma cells (A549)

$ZnSo_4$ conc. (µg/ml)	Viability %	Inhibitory %	S.D. (±)
500	**26.49**	**73.51**	**3.75**
250	**57.08**	**42.92**	**3.14**
125	**81.43**	**18.57**	**1.79**
62.5	**98.12**	**1.88**	**0.46**
31.25	**100**	**0**	
15.6	**100**	**0**	
7.8	**100**	**0**	
3.9	**100**	**0**	
2	**100**	**0**	
1	**100**	**0**	
0	**100**	**0**	

As the quantities of zinc sulphate grew, the cell viability steadily reduced, as shown in Table (5). Against normal lung cell (Wi38), the dose producing 50% cell growth inhibition (IC50) was 463.15µg/ml, as seen in the dose-response curves for cell viability in Figure (3). According to (**Rashad *et al*., 2019**), four different human cell types were treated, including colon cancer (Caco-3), breast cancer (MCF7), lung cancer (A549), and normal lung cell line (Wi38). The viability and morphology of the cells significantly differed between the control and treatment groups, which supported the notion that these elements have a carcinogenic effect.

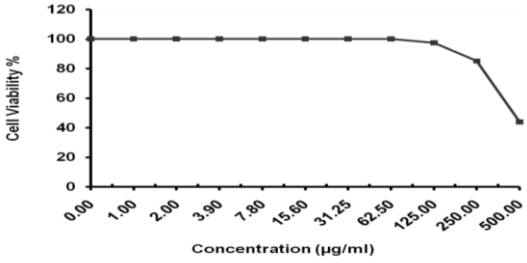

Figure 3: Inhibitory activity of ZnSo4 concentrations against human lung fibroblast normal cells (Wi-38).

Table (5). Effect of different ZnSo4 concentration son human lung fibroblast normal cells (Wi38).

$ZnSo_4$ conc. (µg/ml)	Viability %	Inhibitory %	S.D. (±)
500	**43.87**	**56.13**	**3.69**
250	**85.06**	**14.94**	**2.81**
125	**97.31**	**2.69**	**0.75**
62.5	**100**	**0**	
31.25	**100**	**0**	
15.6	**100**	**0**	
7.8	**100**	**0**	
3.9	**100**	**0**	
2	**100**	**0**	
1	**100**	**0**	
0	**100**	**0**	

2.1. Cell cycle analysis by PI assay using flow cytometry

HepG2 cell DNA composition was impacted by $ZnSo_4$ at doses of 75 µg/ml. The G0/G1 phase for control showed a decline from 44.69% to 41.26%. Similar to the S phase percentage, $ZnSo_4$ and the control both showed a drop from 39.54% to 35.31%. $ZnSo_4$ treatment increased the DNA content of the HepG2 cells in the G2/M phase (23.43%) compared to the control (15.77%), as shown in Table (6). These findings demonstrated a considerable buildup of HepG2 cells in the G2/M phase and demonstrated that $ZnSo_4$ significantly inhibits cell growth by inducing G2/M phase cell cycle arrest as shown in Figure (4).

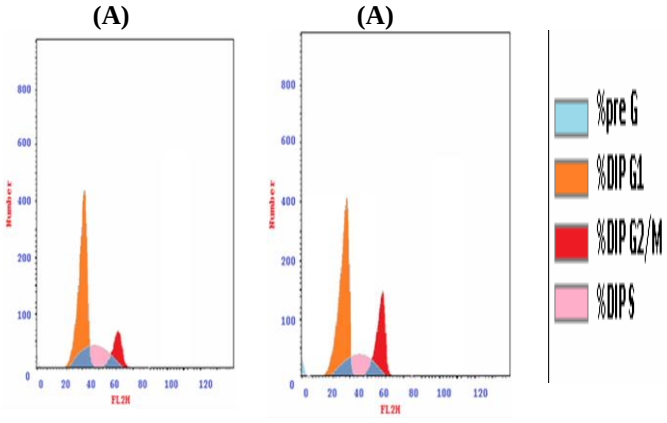

Figure 4: **(A)** liver cancer cell lines (HepG2) - untreated **(B)** Liver cancer cell lines (HepG2) where treated with $ZnSo_4$ at concentration 75µg/ml and effect at G2/M cell cycle arrest.

Table (6): Average % of DNA content in each cell cycle phase using HepG2 cells treated with 75µg/ml of $ZnSo_4$

Groups	Percentages of DNA content each in cell cycle phase			
	G0/G1 phase	S phase	G2/M phase	Pre-G1
HepG2-control	44.69	39.54	15.77	1.64
HepG2-treated	41.26	35.31	23.43	8.92

2.2. Apoptosis analysis by Annexin V-FITC Assay using flow cytometry

The mitochondrial pathway and the caspase cascade are just two of the signalling channels that regulate the closely regulated process of apoptosis. $ZnSo_4$ effects on HepG2 cells were studied in a cell culture to detect cell necrosis and apoptosis at a dosage of 75 µg/ml. Using flow cytometry with Annexin V-FITC/PI double-labeled, apoptosis and necrosis were assessed (Figure 5). The percentage of early and late apoptotic cells was used to compute the apoptotic rate. As can be shown in (Table 7), $ZnSo_4$ treatment of HepG2 cells caused a change in the apoptosis rate, which was 0.84% and 1.83% for both early and late apoptotic cells, respectively. Whereas control values for early and late apoptotic cells were, respectively, 0.43% and 0.15%. When HepG2 cells were treated with $ZnSo_4$, the necrotic impact was 6.25%, compared to 1.06% for control. These findings demonstrated that $ZnSo_4$ had a sizable apoptotic and necrotic effect on HepG2 cells.

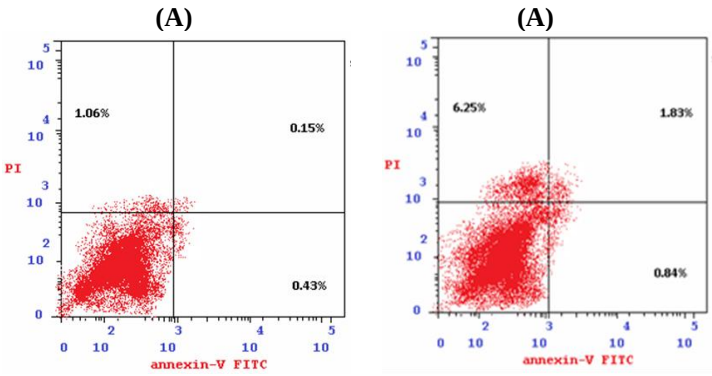

Figure 5: **(A)** liver cancer cell line (HepG2)-untreated **(B)** liver cancer cell line (HepG2) where treated with $ZnSo_4$ at concentration 75µg/ml**. Nt** .Lower left (live cells) - lower right (early apoptosis) -upper right (late apoptosis) - upper left (necrotic cells)

Table (7). Apoptotic and necrotic effect on HepG2 when treated with ZnSo4

Groups	Percentage of apoptosis		Percentage of necrosis
	early	late	
HepG2-control	0.43	0.15	1.06
HepG2-treated with $ZnSo_4$	0.84	1.83	6.25

4. Quantitative RT-PCR analysis

$ZnSo_4$ induced genotoxicity of some related genes, *casp3, Bcl-2* and p^{53} in HepG2 cells

It was investigated how $ZnSo_4$-induced cytotoxicity on HepG2 liver cancer cell lines affected apoptosis. Real-time PCR was used to gauge the expression levels of apoptosis-related genes in HepG2 cells, including *casp3*, *p53*, and *Bcl-2* (qRT-PCR). *Casp3* increased by 3.12285797 points more than the control (Table 8), while *p53* rose by 2.577512 points more than usual (Table 8). *Bcl-2* reduced by 0.6682521 compared to control (Table 9), which demonstrated that the expression levels of the *p53* and *casp3* genes were higher in the treated group than in the control group (Table 10). In contrast, the expression level of the *Bcl-2* gene was lower (Figure 6). These findings showed that $ZnSo_4$ killed HepG2 cells primarily via up-regulating *casp3* and *p53* genes during apoptosis, while down-regulating *Bcl-2*.

Table (8): Effect of ZnSo4 compound administration on the relative expression of casp3 gene in HepG3 cells.

Groups	*Casp3*Ct values	Δ Ct	ΔΔ Ct	Relative quantification
Control HepG2	**33.88**	**10.2**	**0.00**	**1.00**
Treated HepG2	**31.32**	**8.39**	**-1.78**	**3.122857**

Table (9): Effect of ZnSo4 compound administration on the relative expression of p53 gene in HepG3 cells.

Groups	p^{53}Ct values	Δ Ct	ΔΔ Ct	Relative quantification
Untreated HepG2	**33.08**	**9.37**	**0.00**	**1.00**
Treated HepG2	**30.82**	**7.89**	**-1.48**	**2.577512**

Table (10): Effect of ZnSo4 compound administration on the relative expression of Bcl-2 gene in HepG2 cells.

Groups	*Bcl-2* Ct values	Δ Ct	ΔΔ Ct	Relative quantification
Untreated HepG2	**28.51**	**4.8**	**0.00**	**1.00**
Treated HepG2	**28.36**	**5.43**	**0.36**	**0.6682521**

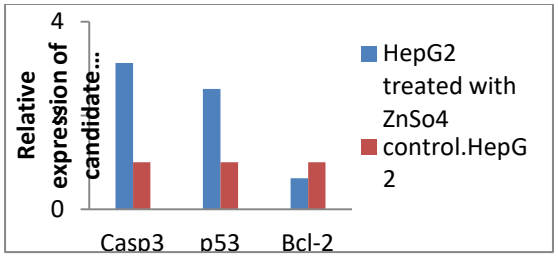

Figure 6: Effects of ZnSo4 on apoptosis-related genes after exposure to 75µg/ml, mRNA expression of casp3, p53 and Bcl-2 was assessed by quantitative RT-PCR *P < 0.05, compared to the control group.

5. Toxicity to (YKO) strains tested with Zinc sulphate by comet assay

According to the comet assay, zinc sulphate had variable degrees of yeast-specific genotoxic effects on YKO. The genotoxic effects of $ZnSo_4$ at doses of (50, 75, and 100 µg/ml) were discovered. The *MMT1* gene was less genotoxic than other genes, however the *CLN1*, *MRE11*, and *ZRC1* genes had strong genotoxic effects. Table provided the distribution of the determined comets for zinc sulphate (11).

It should be noted that for each of the four tested genes, the yeast predicted noticeably more comets than the control (Figure 7), showing that the tested $ZnSo_4$ caused numerous deoxyribonucleic acid damages. It was evident from the cells that each of the four genes had been significantly damaged by zinc sulphate treatment evaluated.

Table (11): Image analysis of comet assay parameters in cells of all groups after $ZnSo_4$ treatment.

Concentrations	**Tail Length (px)**	**Tail DNA (%)**	**Tail Moment**	**Tail Olive Moment**
ControlMMT1 (A)	3.2	16.42885	0.856675	1.331495
50 µg/ml (A1)	5.84	18.56993	2.698397	2.569634
75 µg/ml (A2)	7.96	24.76888	3.678652	3.649392
100 µg/ml (A3)	10.9	26.52228	5.214025	4.659043
ControlCLN1 (B)	4.14	17.84848	1.408786	2.093441
50 µg/ml (B1)	7.02	21.30251	2.494028	3.093563
75 µg/ml (B2)	9.7	30.84848	3.890823	4.417296
100 µg/ml (B3)	15.86275	38.18079	8.828677	6.79219
ControlMRE11 (C)	3.7	11.32471	0.644259	1.424435
50 µg/ml (C1)	5.74	18.33586	1.895839	2.269366
75 µg/ml(C2)	9.66	26.86337	4.662948	4.175398
100 µg/ml (C3)	17.48	30.11288	9.030276	6.586223
ControlZRC1 (D)	4.510204	15.1704	0.988069	1.662803
50 µg/ml(D1)	7.627451	23.06511	3.322405	4.314785
75 µg/ml(D2)	12.08	25.41651	6.076189	5.287539
100 µg/ml(D3)	18.66	38.52412	10.73177	8.686483

Different superscript letters in the same column of tail length showed significance difference at P<0.05.

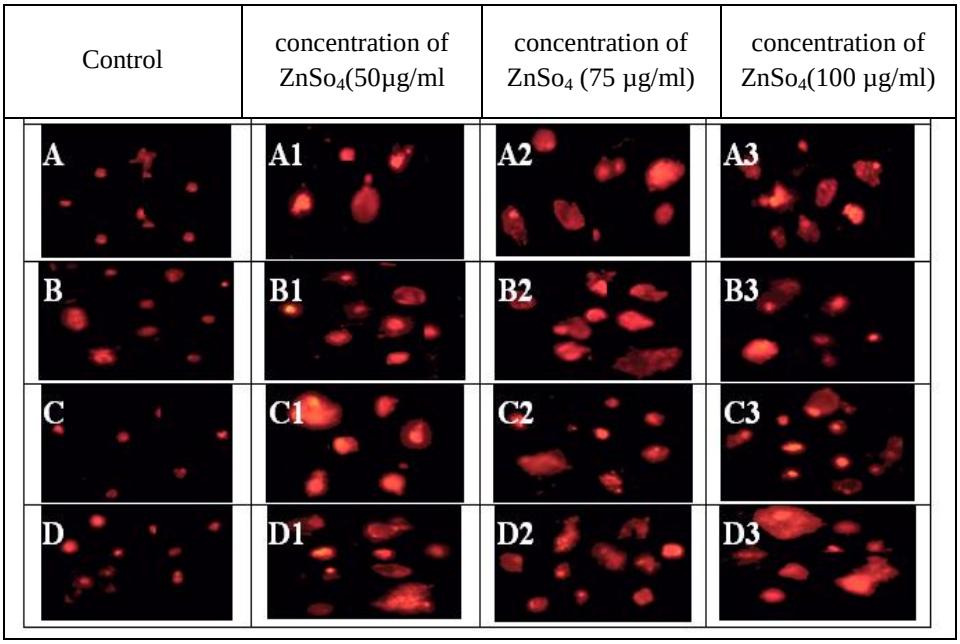

Figure 7: Photomicrographs showing DNA damage in yeast strains using the Comet assay and Zink sulphate at a dose of (50, 75, 100 µg/ml). Control cells A: control *MMT1* gene; A1, A2, A3: treated *MMT1* gene; B: control *CLN1* gene; B1, B2, B3: treated *CLN1* gene; C: control *MRE11* gene; C1, C2, C3: treated *MRE11* gene; D: control *ZRC1* gene; D1, D2, D3: treated *ZRC1* gene.

3.4. Selection of yeast haploid strains devoid of genes similar to specific human cancer genes in vitro.

Sequence similarity comparisons between human and yeast sequences were used to establish the genotypes of haploid (knockout) yeast strains.

The outcomes of an alignment between the yeast *MMT1* and human *SLC30A9* sequences are shown in Figure (8). *MMT1* Putative metal transporter thought to be involved in the buildup of iron in the mitochondria; *MMT1* has a paralog, *MMT2*, which resulted from whole-genome amplification.

```
NC_001145.3:MMT1        ----------------------------------------AAATTGAAAAGGCTGCAATAA  208
NC_000004.12:SLC30A9    CTGTCTCAAAAAAAAAAAAAAAGAAAAAGAAAAAGGTGGAGGAAAAAGTGCCTGCAGAGG  50319
                                                                *..::.**.:* *****.:..

NC_001145.3:MMT1        AG------------------GAATTGGAGAA--AAATCCTC--------AATACCAAAAA  240
NC_000004.12:SLC30A9    AGATTGAGGAGGAGTAAGGAGAAAAGTAGAAAGAAAACCAGGAGTGTATTAGTCCATTTT  50379
                        **                  ***:** ****  ***:**:         :* :***::::

NC_001145.3:MMT1        TTAGCTGAAGC-------ATTCAACAGTCATGATCATGTTCATT--------------TA  279
NC_000004.12:SLC30A9    CACGCTGCTGATAAAGACATACCCAAGACTGGGCAATTTACAAAAGAAAGAGGTTTAATT  50439
                         :.****.:*.       **:*...**:*: *. .** *:**::             *:

NC_001145.3:MMT1        CGTGAATCAGAGACCGAGCAAAA---CGACATAATTTCATTG-----G----------GC  321
NC_000004.12:SLC30A9    GGACTTACAGTTCCCGTGGCTAGGGAAGCCTCACAATCATGGTGGAAGGCAAGGAGGAGC  50499
                         *: :::***: .***:* .:*.   .*.*: *.::**** *     *          **

NC_001145.3:MMT1        ACGATACGAGACTACA----A---AAGCAGTAAATGTGAGCAA--GCTGATAAGCCTTCG  372
NC_000004.12:SLC30A9    AAGTTA--TGTCTTACATGGATGGCAGCAGGCAAATAGAGCTTGTGCAGGGTAACTCCCA  50557
                        *.*:**  :*:**:..    *   .***** .**: :****::  **:*. :*.*   *.

NC_001145.3:MMT1        TCGTT--GAATCTG-------C--ATTCGCATACACATTCTCATGGAC----------AT  411
NC_000004.12:SLC30A9    TTTTTAAAAACCATCACATCTCATGAGCTCATTCACTATCACAAGAACAACATGGGAAAG  50617
                        *  **  .** *:        *  .: * ***:***::**:**:*.**          *

NC_001145.3:MMT1        ACGCATTCTCATGCTGCTCACA----------------ATCCATTATTAGTACTTAGT-A  454
NC_000004.12:SLC30A9    ACCCACCCTCATGCTTCAGTCATCTCCCACTGCGTCCCTCCCAAAACATGTGGGAATTAT  50677
                        ** **  ******** *: :**                : ***::* ::**.  :* * :

NC_001145.3:MMT1        CTGAGCAAATT--AGGAAAAATGCAGGCG----------TAAGAATCACATGGGTCGG--  500
NC_000004.12:SLC30A9    AGGAGCTACAAGATGAGATTTTGTGGGAGACACAGAGCCAAACCATATCAAGGAGTGTCA  50737
                        . ****:*.::  :*..*:::** .**.*          :** .**.:**:**.  *

NC_001145.3:MMT1        -------CTTAGGTGTAAACGTTGGTATTGCTATAGGTAAATTTTTTGGAGGTATCGTAT  553
NC_000004.12:SLC30A9    AGAAAGCCAAGGGAAGAAGCGTTTGTTT----------TTTTT--TTGTGAGACGGAAT  50784
                               *:.**:. **.**** **:*           ::***  * *:*. *  *:**
```

Figure 8: Gene alignment between human gene *SLC30A9* and the yeast *MMT1* in the Clustal Omega web site ('*' indicates identical between two aligned, '-' indicates gaps missing of one) and ('.' indicates low similarity, ':' indicates more similarity used to denote the level of similarity that are not identical) at position.

The outcomes of an alignment between the human *CCNA1* and yeast *CLN1* sequences are shown in Figure (9). The G1 cycle is involved in controlling the cell cycle; it activates Cdc28p kinase to promote the G1 to S phase transition; late G1-specific expression depends on the MBF (Swi6p-Mbp1p) and SBF (Swi6p-Swi4p) transcription factor complexes; *CLN1* has a paralog, *CLN2*, which emerged from whole genome duplication; the cell cycle arrest phenotype of any of human cyclins *CCNA1*, *CCNA2*, *CCNB1*, *CCNC*, *CCND1* or *CCNE1*.

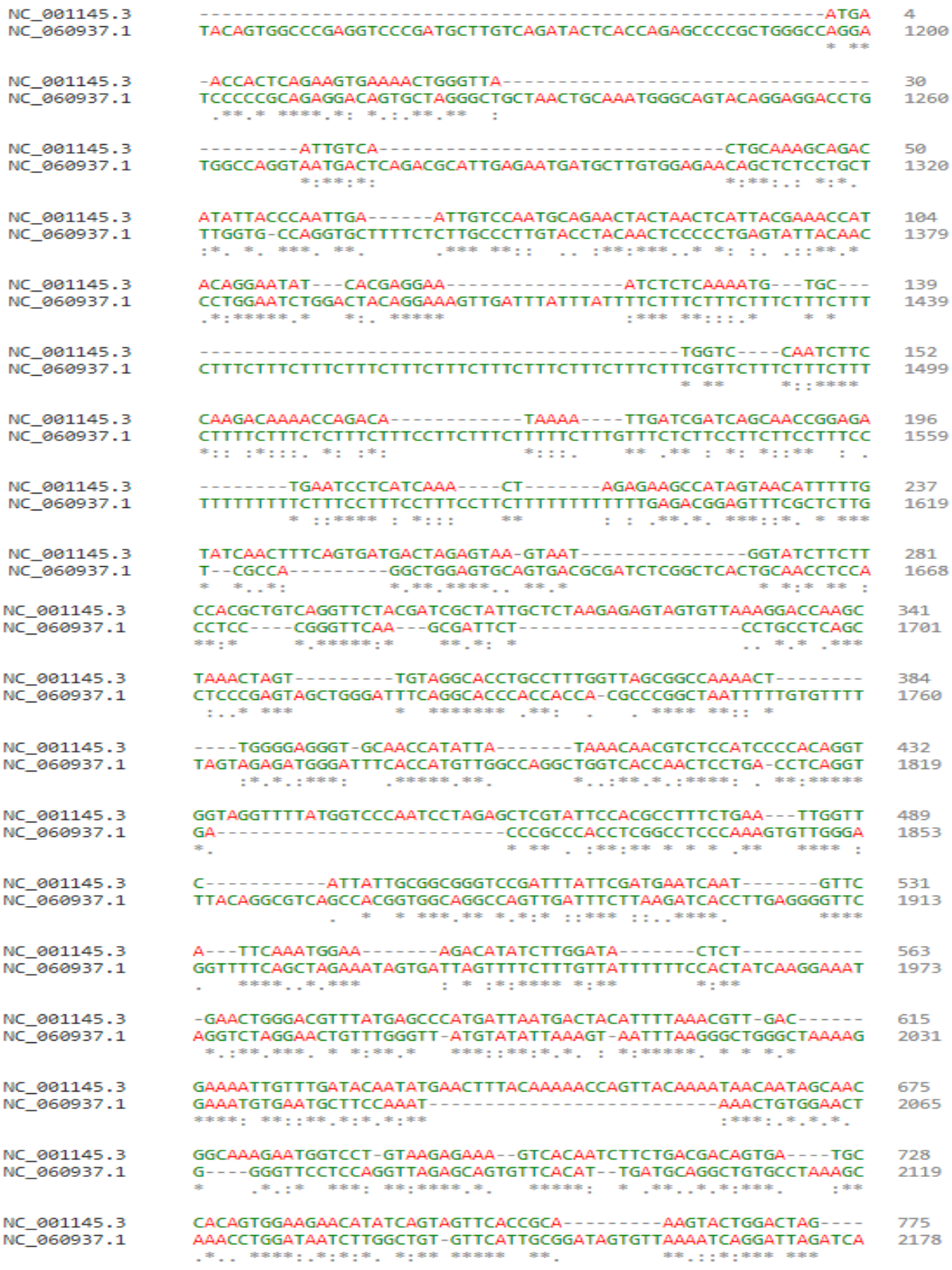

Figure 9: Gene alignment between human gene *CCNA1* and yeast *CLN1* gene in the Clustal Omega web site ('*' indicates identical between two aligned, '-' indicates gaps missing of one) and ('.' indicates low similarity, ':' indicates more similarity used to denote the level of similarity that are not identical) at position.

Figure (10) demonstrates the outcomes of alignment between yeast and human *MRE11* sequences. Mre11p wants to associate with Ser/Thr-rich ORFs in the premeiotic phase; nuclease activity is necessary for MRX function; it is widely maintained and forms nuclear foci in response to DNA replication stress. *Mre11p* is a nuclease subunit of the MRX complex with *Rad50p* and Xrs2p. The MRX complex performs in repair of DNA double-strand break times and in telomere stability.

Figure 10: Gene alignment in the Clustal Omega web site between human gene *MRE11* and yeast gene *MRE11* ('*' indicates identical between two aligned, '-' indicates gaps missing of one) and ('.' indicates low similar, ':' indicates more similar used to denote the level of similarity that are not identical) at position.

Figure (11) showed the results of alignment between the human *SLC30A10* and yeast *ZRC1* sequences. Vacuolar cell wall zinc transporter; transports zinc from cytosol to vacuole for storage; also contributes to resistance to zinc shock caused by sudden influx of zinc into cytoplasm; human ortholog *SLC30A10* serves as a Mn transporter; genetic changes in *SLC30A10* cause neurotoxic deposition of Mn in the liver and brain; *ZRC1* has a paralog, *COT1*, which emerged from the whole genome duplication.

Figure 11: Gene alignment in the Clustal Omega web site between human gene *SLC30A10* and yeast gene *ZRC1* ('*' indicates identical between two aligned, '-' indicates gaps missing of one) and ('.' indicates low similar, ':' indicates more similar used to denote the level of similarity that are not identical) at position.

3.5. Yeast protein-protein interaction prediction (Networking).

The degree of purposeful similarity between two eucaryotes' cancer-related genes could be determined by predicting the interactions between proteins in yeast and humans (Figures 12). Every data set chosen for the investigation is shown in Gene MANIA together with its prognostic value. Currently, separate sequencing execution prediction approaches on yeast and humans are provided in addition to or above two organisms (*Homo sapiens* and *Saccharomyces cerevisiae*). Sequence MANIA is a useful tool for any scientist because to the GeneMANIA predictive algorithmic program's exceptional accuracy, Associate in Nursing perceptive computer programmers, and depth of knowledge. (**Rashad *et al.*, 2021**).

GeneMANIA is presenting four yeast queries (Fig. 12). Four distinct relevant yeast genes that are connected by a pathway to the query list and many totally different absolutely different interactions result in fully distinct networks. Other levels of question customisation include physical interaction (48.13%), co-expression (6.89%), predicted (4.47%), co-localization (2.10%), other (1.02%), genetic interaction (36.83%), shared protein domains (0.34%) and pathway (0.22%) common. Results from gene queries are shown in Impacts of Knowledge Set Selection on Topology by GeneMANIA. Mistreatment of the yeast basic question's default settings. A yeast default question is the misuse default network weight technique.

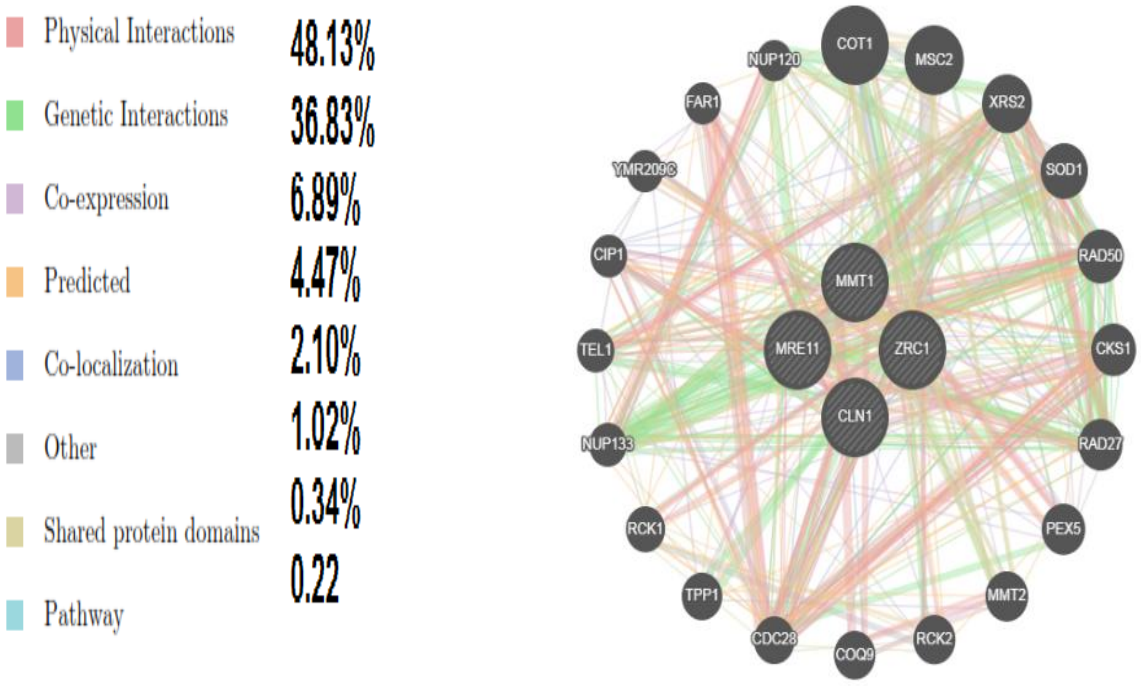

Figure 12: The yeast cell-cycle default query with all default parameters. The yeast cell-cycle default query with all default parameters. Using the default network weighting approach, the yeast cell-cycle default query.

GeneMANIA is presenting four human queries (Fig. 13). Four distinct relevant human genes that are connected by a pathway to the query list and many totally different absolutely different interactions result in fully distinct networks. Other levels of question customisation include physical interaction (77.64%), co-expression (8.01%), predicted (5.37%), co-localization (3.63%), other (1.02%), genetic interaction (2.87%), shared protein domains (0.60%) and pathway (1.88%). Results from gene queries are shown in Effects of Knowledge Set Choice on Topology by GeneMANIA.A human default question, mistreatment default network weight approach. We selected YKOs deficient in genes related to human cancer genes. Predicting protein-protein interactions in yeast and humans may make it possible to gauge how deliberately similar certain cancer-related genes are in the two species.

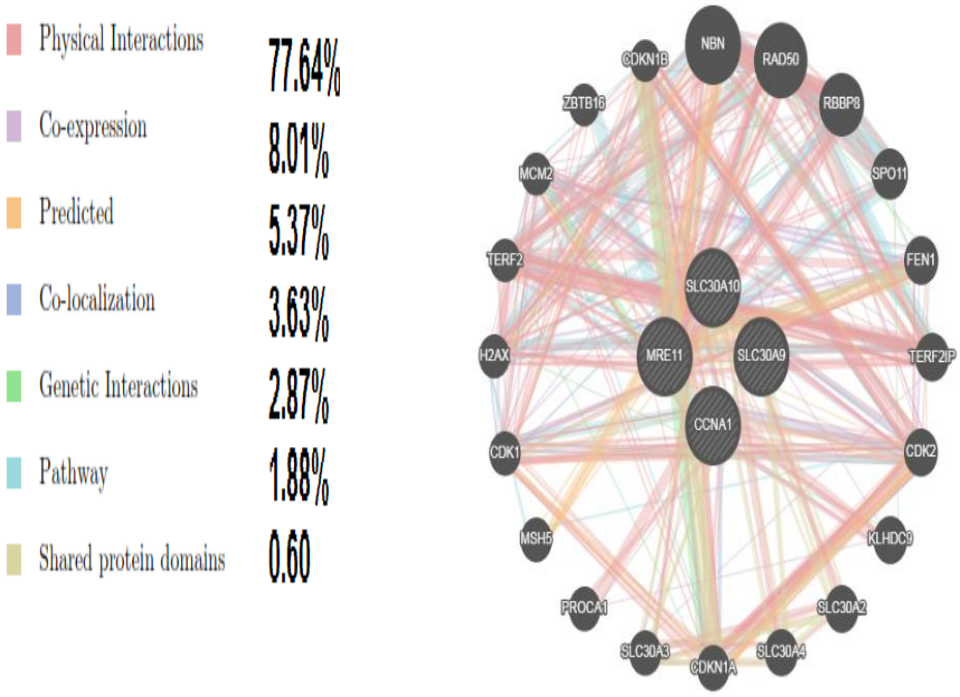

Figure 13: The human default query, using all default parameters. The human default query, using default network weighting method.

4. Conclusions

The cell survival of A549 initially rose and then reduced with increasing zinc concentration, with the turning point happening at 50 mM $ZnSo_4$, similarly to **Yuan *et al.* (2012).** The viability of the A549 cells was finally reduced by a greater zinc concentration (75 mM). Additionally, **Wang *et al.* (2013)** reported that after 48 hours of treatment, HepG2 cell viability reduced as $ZnSo_4$ concentration increased. According to **Wang *et al.* (2016),** MDAMB231 cells' viability dropped to 80% after being exposed to 50 µM $ZnSo_4$ for 24 hours. $ZnSo_4$-treated cells had a considerable rise in intracellular zinc concentration, which caused cell death. **Zhao *et al.* (2015)** demonstrated that higher $ZnSo_4$ concentrations lowered the viability of A549 cells, even if the viability of A549 cells remained between 50% and 20% after being treated with 500 µM $ZnSo_4$ for the indicated times for 9 and 24 h, respectively. The findings of this

analysis are consistent with those found in **Cui *et al*. 2002.** They discovered that HepG2 cells' cell cycle progression was easily affected by a low intracellular zinc status. ZD cells were shown to have a high fraction of G1 cells, and zinc depletion significantly decreased the number of cells in the S phase. It has been reported that zinc is essential for HepG2 cells to advance from the G1 to the S phase. Uncertainty persists regarding the mechanism by which zinc deficiency hinders the G1 to S phase transition. Zinc depletion resulted in a decrease in the amount of DNA on each plate, which is consistent with earlier research with HepG2 cells. Cui *et al*. added just 0.4 µM zinc dramatically increased the DNA content per plate, demonstrating that even small changes in cellular zinc status had a large impact on DNA synthesis and cell proliferation. On the other hand, it's possible that some of the lithium HepG2 cells were going through apoptosis because of the decreased DNA content caused by zinc depletion (**Nakatani *et al* 2000**).

The vitality of liver cancer (HepG2) cells was inhibited by flow cytometry analysis, thus it was important to evaluate the cytotoxic impact of food additives on cell cycle arrest-based cell cycle distribution. The findings demonstrated a considerable buildup of HepG2 cells in the G2/M phase and demonstrated that additives have lethal effects by causing cell cycle arrest in the G2/M phase (**Rashad *et al*., 2022**).

Kocdor *et al.*, (2015) showed that the zinc cytotoxicity in p53-wild lung cancer cells but not in null cells at different supra physiological concentrations. Suggested that many cytotoxic molecules induce mitotic cell death (apoptosis) which occurs in parallel with G2/M arrest.

Rashad *et al*., 2018 reported that the mRNA levels of the *p53*, *Bax*, and *Bcl-2* genes were determined using the quantitative real time-PCR method. The information demonstrated that these associated genes' transcriptional levels were altered by dietary additives. *P53* and Bax mRNA expression was increased, however *Bcl-2* transcription was dramatically down regulated compared to the control.

The current data show that $ZnSo_4$ activated *p53* and reduced *Bcl-2*, which in turn activated downstream molecular pathways controlled by mitochondria, including *caspase3* activation. In conclusion, HepG2 cells can efficiently undergo apoptosis when treated with ZnSo4. $ZnSo_4$ activated a caspase cascade mediated by the mitochondria and inhibited the anti-apoptotic protein *Bcl-2* to induce apoptosis. $ZnSo_4$ is also thought to be cytotoxic for HepG2 cells at concentrations of (50, 75, 100 µg/ml) but not for normal Wi-38. Higher than this concentration reduced both cancerous and non-cancerous cells' viability and established the presence of their cytotoxic effects.

5. Conflicts of interest

"There are no conflicts to declare".

6. Acknowledgments

We truly appreciate the two senior reviewers' insightful remarks and constructive criticism.

References

[1] Barbier O., Jacquillet G., Tauc M., Cougnon M., Poujeol P. (2005). Effect of heavy metals on, and handling by, the kidney. *Nephron Physiology*, 99, 105.

[2] Costello L.C. and Franklin R.B. (2016). A comprehensive review of the role of zinc in normal prostate function and metabolism; and itsimplications in prostate cancer. *Arch BiochemBiophys* 611:100– 112. https://doi.org/10.1016/j.abb.2016.04.014

[3] Cui, L., Schoene, N. W., Zhu, L., Fanzo, J. C., Alshatwi, A., and Lei, K. Y.(2002). Zinc depletion reduced Egr-1 and HNF-3 expression and apolipoprotein A-I promoter activity in HepG2 cells. *Am J Physiol Cell Physiol* 283: C623–C630 https://doi.org/10.1152/ajpcell.00308.2001.-We

[4] KLUG A. (2010): The discovery of zinc fingers and their applications in gene regulation and genome manipulation. *Annual Review in Biochemistry*, 79, 213-24.

[5] Kocdor H., Ates H., Aydin S., Cehreli R.,Soyarat F., Kemanli P., Harmanci D., Cengiz H., and Kocdor MA.,(2015): Zinc supplementation induces apoptosis and enhances antitumor efficacy of docetaxel in non-small-cell lung cancer. *Drug Design, Development and Therapy* 2015:9 3899–3909

[6] Livak, K. J., & Schmittgen, T. D. (2001). Analysis of relative gene expression data using real-time quantitative PCR and the 2(−Delta Delta C(T)) method. *Methods*, 25, 402–408.

[7] Marcinčáková, D., Schusterová, P., Mudroňová, D., Csank, T., Falis, M., Fedorová, M., Marcinčák, S., Hus, K. K., andLegáth, J. (2019). Impact of zinc Sulphate exposition on viability, proliferation and cell cycle distribution of epithelial kidney cells.*Polish Journal of Environmental Studies*, 28(5), 3279–3286.https://doi.org/10.15244/pjoes/94045

[8] McCord MC, Aizenman E (2018). The role of intracellular zinc release in aging, oxidative stress, and Alzheimer's disease. Front Aging Neurosci 6:1–16. https://doi.org/10.3389/fnagi.2014.00077

[9] Mousaa S. A., Abdel Hamid A. Haggran, Tahany M. A. El-kawokgy, Zakia A. Abou-El-Khier, Shadia M.Sabry, Shimaa E. Rashad (2022). Impact assessment of cadmium chloride on human cell lines and yeast knockout strains. Egyptian Pharmaceutical Journal Vol 21, issue (4).

[10] Nakatani T, Tawaramoto M, Opare Kennedy D, Kojima A, and Matsui-Yuasa I. (2000). Apoptosis induced by chelation of intracellular zinc is associated with depletion of cellular reduced glutathione level in rat hepatocytes. *ChemBiol Interact* 125: 151–163

[11] Nazıroğlu M, Yürekli VA (2013): Effects of antiepileptic drugs on antioxidant and oxidant molecular pathways: focus on trace elements. Cell MolNeurobiol 33:589–599

[12] Plum, L. M.; Rink, L.; Haase, H. (2010): The essential toxin: Impact of zinc on human health. *International Journal of Environmental Research and Public Health*, 7 (4): 1342-365

[13] Rashad Sh. E., A. A. Haggran, E. I. Aboul-Elab, A. H. Shaalan, A. S. S. Abdoon (2022). Cytotoxic and genotoxic effects of 50nm Gold Nanorods on mouse splenocytes and human cell lines. *Egypt. J. chem.*, Article in Press. 10.21608/EJCHEM.2022.134210.5914

[14] Rashad Sh. E., F. M. Abdel-Tawab, Eman M. Fahmy, AG. Attalla, E. S. Ahmed and A. A. Haggran (2018). Determination of genotoxic effects of some food additives on some human cancer cells by flow cytometry analysis. *Egypt. J. Genet. Cytol.*, 47:329-343.

[15] Rashad Sh. E., F. M. Abdel-Tawab, Eman M. Fahmy, AG. Attalla, Ekram S. Ahmed and A. A. Haggran (2019). Assessment of genotoxic effects of some food additives on some human cancer cells. *AUJAS, Ain Shams Univ., Cairo, Egypt, Special Issue*, 27(1). DOI: 10.21608/AJS.2019.43668

[16] Rashad Sh. E., F. M. Abdel-Tawab, Eman M. Fahmy, AG. Attalla, Ekram S. Ahmed and A. A. Haggran (2021). Application of the yeast comet assay in testing some food additives for genotoxicity by comet assay in yeast. *Egypt. J. chem., Issue,* 64: (12) 7649-7667. 10.21608/EJCHEM.2021.90428.4315

[17] Silvera SAN, Rohan TE (2007): Trace elements and cancer risk: a review of the epidemiologic evidence. *Cancer Causes Control*, 18:7–27

[18] Sliwinski, t.; czechowska, a.; kolodziejczak, m.; jajte, j.; jarosinska, m. W.; blasiak, j. (2009): Zinc salts differentially modulate DNA damage in normal and cancer cells. *Cell Biology International*, 33(4): 542-547.

[19] Vermes, I., Haanen, C., Steffens-N., H., Reutellingsperger, C., (1995). A novel assay for apoptosis Flow cytometric detection of phosphatidylserine expression on early apoptotic cells using fluorescein labelled Annexin V. *Journal of Immunological Methods*, 184 (1), 39-51.

[20] Wang, Y. H., Li, K. J., Mao, L., Hu, X., Zhao, W. J., Hu, A., and Zheng, W. J. (2013): Effects of exogenous zinc on cell cycle, apoptosis and viability of MDAMB231, HepG2 and 293 T cells. *Biological Trace Element Research*, *154*(3), 418–426. https://doi.org/10.1007/s12011-013-9737-1

[21] Wang, Y. hong, Zhao, W. jie, Zheng, W. juan, Mao, L., Lian, H. zhen, Hu, X., &Hua, Z. chun. (2016): Effects of Different Zinc Species on Cellar Zinc Distribution, Cell Cycle, Apoptosis and Viability in MDAMB231 Cells. *Biological Trace Element Research*, 170(1), 75–83. https://doi.org/10.1007/s12011-015-0377-5

[22] Xie, H., Holmes, A. L., Young, J. L., Qin, Q., Joyce, K., Pelsue, S. C., Peng, C., Wise, S. S., Jeevarajan, A. S., Wallace, W. T., Hammond, D., & Wise, J. P., Sr (2009). Zinc chromate induces chromosome instability and DNA double strand breaks in humanlung cells. *Toxicology and appliedpharmacology*, 234(3),293–299. https://doi.org/10.1016/j.taap.2008.10.010

[23] Yehy.h., lee y.t., hsiehy.l., and hwangd.f. (2011): Dietary taurine reduces zinc-induced toxicity in male wistar rat. *Journal of Food Science*, 76, T90-T98.

[24] Yuan, N., Wang, Y. H., Li, K. J., Zhao, Y., Hu, X., Mao, L., andZheng, W. J. (2012): Effects of exogenous zinc on the cellular zinc distribution and cell cycle of A549 cells. *Bioscience, Biotechnology and Biochemistry*, 76(11), 2014–2020. https://doi.org/10.1271/bbb.120216

[25] Zaman, M., Johnson, A., Petersingham, G., Muench, G., Dong, Q., and Wu, Ming. (2019). Protein kinase CK2 is involved in zinc homeostasis in breast and prostate cancer cells. *BioMetals*. 32. 10.1007/s10534-019-00218-z.

[26] Zhang X., Wang Z., Mao L., Dong X., Peng Q., Chen J., Tan C., Hu R. (2017): Effect of ZnO nanoparticle on cell viability, zinc uptake efficiency, and zinc transporters gene expression: a comparison with ZnO and $ZnSo_4$. Czech J. Anim. Sci., 62, 32–41

[27] Zhao, W. J., Song, Q., Zhang, Z. J., Mao, L., Zheng, W. J., Hu, X., &Lian, H. (2015). The kinetic response of the proteome in A549 cells exposed to $ZnSo_4$stress. *PLoS ONE*, 10(7), 1–21. https://doi.org/10.1371/journal.pone.0133451

[28] Zodl b., zeiner m., sargazi m., robertsn.b., marktl w., steffani., ekmekcioglu c. (2003). Toxic and biochemical effects of zinc in CaCo-2 cells. *Journal of Inorganic Biochemistry*, 97, 324-330.